



Experimental characterization of in-plane behaviour of old masonry walls strengthened through the addition of CFRP reinforced render

João Guerreiro^{a,*}, Jorge Proença^b, João Gomes Ferreira^b, António Gago^b

^a Ceris Research Fellow, Instituto Superior Técnico – Universidade de Lisboa (IST-UL), Lisbon, Portugal

^b Department of Civil Engineering and Architecture, IST - UL, Lisbon, Portugal

ARTICLE INFO

Keywords:

Masonry walls
In-plane loads
Seismic strengthening
Reinforced render
CFRP mesh

ABSTRACT

This article presents the results of an extensive experimental programme investigating the structural performance for in-plane loads of old masonry walls strengthened using a specific technique that consisted of applying a CFRP mesh embedded within a shotcreted render. In this article the expression old masonry refers to rubble stone masonry with lime-based mortar but it is believed that the strengthening technique can also be applied to other types of old masonry (e.g. solid or almost solid clay or concrete brick masonry).

The reinforcing composite material, called CFRP reinforced render (CFRP-RR), is characterized by the use of a CFRP mesh and the shotcreted pre-mixed mortar, lime-based, specific for the rehabilitation of old masonry load bearing walls. This material is applied to one or both faces of the masonry walls, thus improving both the in-plane and out-of-plane behaviour for horizontal loads (the latter benefits are described in Ref. [1]).

The experimental programme consisted of the in-plane testing of full-scale physical models of walls, herewith called specimens. These were subjected to reversed cyclic horizontal loads (simulating earthquake loads) with constant vertical loads (simulating gravity loads). The comparison between the experimental results of the non-reinforced with the reinforced (strengthened) specimens allowed the quantification of the inherent benefits in terms of structural performance under earthquake actions.

1. Introduction

The strengthening technique described in the present article was developed by a private company specialized in the conservation and retrofitting of old constructions with the scientific support of CERIS (www.ceris.pt). It was initially conceived with the purpose of preventing the out-of-plane collapse of masonry walls in old buildings.

The out-of-plane collapse mechanisms of masonry walls mainly occur due to their bending shortcomings, caused by the residual tensile strength of the masonry material [2–4]. On the other hand, when masonry walls are subjected to in-plane loads there is an interaction between shear and bending (i.e., rocking) which causes diagonal and horizontal cracking [5–8].

For masonry buildings, satisfactory seismic behaviour will be achieved if the out-of-plane collapse is prevented, the walls subjected to in-plane loads have the required strength and both these sets of walls are effectively interconnected. For non-reinforced masonry walls, the critical mechanism is often the out-of-plane collapse, since the walls subjected to in-plane forces are more reliable in an earthquake as they do not immediately collapse when they start to manifest the previously

mentioned damage patterns [9–11]. Despite some restrictions, the horizontal inertia forces in these walls can still be transmitted long after the diagonal or horizontal cracks appear.

Fibre reinforced polymers (FRP) has nowadays considerable interest for application to the seismic strengthening of old buildings provided from their high strength to weight ratio, thinner cross-sections, non-corrosive nature of constituent materials and a diversified application [12–15]. Recent research on the strengthening of old masonry walls using polymeric materials (FRP) have generally pointed to using strips of these materials (glass or carbon fibre based), while ensuring their bonding by organic adhesion through the use of resins, usually epoxide, e.g. Refs. [16–20].

The preservation of the permeability characteristics of the façades of old buildings should also be considered when developing a strengthening technique. Degrading their physical and mechanical characteristics by waterproofing the external layer of the façade threatens the durability of the overall structural solution. References to other adhesion methods or agents are relatively scarce, e.g. Refs. [21,22], since it has been shown that it is difficult to take full advantage of the reinforcing material without resorting to organic bonding.

* Corresponding author.

E-mail addresses: jg@civil.ist.utl.pt (J. Guerreiro), jorge.m.proenca@tecnico.ulisboa.pt (J. Proença), joao.gomes.ferreira@tecnico.ulisboa.pt (J.G. Ferreira), antonio.gago@tecnico.ulisboa.pt (A. Gago).

<https://doi.org/10.1016/j.compositesb.2018.04.045>

Received 4 December 2017; Received in revised form 30 March 2018; Accepted 20 April 2018
Available online 22 April 2018

1359-8368/ © 2018 Elsevier Ltd. All rights reserved.

To overcome the previously identified limitation some studies have been carried out recently with a composite reinforcing material, externally applied onto the existing masonry, bearing some similarities with CFRP-RR [23–26]. This other material is normally identified by FRCM (Fabric, or Fibre, Reinforced Cementitious Matrix). Similarly, to CFRP-RR, the fibres of the FRCM (e.g., carbon, glass, basalt and others) are intended to compensate the effects of the lack of tensile strength of the masonry wall material [27].

The main characteristics of CFRP-RR are described in Ref. [28] and can be summarized as follows: (i) the matrix of the composite material is based on renders specially developed for rehabilitation of old masonry buildings; (ii) the strengthening material is carbon-fibre based; (iii) the application procedure (shotcreting) is intended to maximize the exploration of the unique properties (high strength) of the strengthening material, as well as to improve the adhesion to the underlying masonry wall material; and (iv) the applicability has been directed to rubble stone masonry (as opposed to clay brick masonry). Specific lime based mortars are beginning to be widely used in conservation works involving old masonry because of their compatibility with the substrate, due to their similar composition. These mortars are made exclusively from natural hydraulic or air lime and have particular thixotropic properties, as well as adhesion, chemical resistance and durability, better adapted to the intended application. The increase in demand has led to premixed mortars becoming more widely commercially available. Their coherent mechanical strength and stiffness, high vapour permeability and low content of soluble salts, constitute excellent characteristics for the bonding to the masonry substrate.

2. Description of the strengthening technique

The developed strengthening technique consists of applying a CFRP reinforced render to the masonry wall's substrate (Fig. 1a). A layer of this nature has high tensile strength and good capacity to bond to the original masonry substrate, thus providing the masonry with improved bending resistance.

The reinforced render can be described as a bi-component material, composed of a hydraulic but non-cementitious coat mortar and a carbon fibre reinforced polymer (CFRP) mesh. The coat mortar's function is to bond the reinforcement layer to the masonry wall, as it keeps chemical, physical and mechanical compatibility with the ancient masonry. On the other hand, the CFRP mesh will provide the reinforcement layer with the necessary tensile strength.

The main advantages [22] of using CFRP mesh instead of traditional steel meshes derive essentially from its higher tensile strength, durability, ease of application, and thinner mortar layer (unlike steel meshes, CFRP mesh does not require a mortar cover to protect it from the environment).

The results of preliminary tests [28] showed that a traditional mortar coating application was not able to ensure proper bonding between the reinforcing mesh and the matrix of the reinforced render when the CFRP mesh resistance is fully exploited. On the contrary, the works of Carozzi et al. [25] with a comparable material (FRCM) showed

that it is possible to fully exploit the tensile capacity of the reinforcing mesh.

Consequently, a novel application technology was then developed, based on shotcrete technology, to ensure the necessary bonding (Fig. 2). Because the coat mortar is applied by high-speed spraying to the masonry substrate, this safeguards the adhesion levels [29] needed to bond the reinforced render material to the masonry substrate [21,30]. The foreseeable application of the CFRP reinforced render should comprise the following three stages: (i) removing the wall coating and roughening of the wall surfaces and mortar joints; (ii) positioning and stretching of the CFRP mesh over the wall surfaces; (iii) shotcreting with lime-based mortar.

To prevent the detachment of masonry leaves as a result of the combined effect of compression and bending, especially when the connection between leaves is poor or non-existent [31–33], the strengthening technique also takes into account the connection between both sides of the masonry walls through the installation of steel confinement devices. Those steel confinement devices, when properly placed, also ensure an enhanced bonding between the strengthening layer and the masonry wall, thus increasing the benefits that result from the resource to a high-strength tensile material such as the CFRP.

Anchoring at singular zones is fundamental to ensure the satisfactory overall behaviour of the strengthening layer. This layer will only be effective if properly anchored at its endings, as well as at specific transitional zones where the layer is interrupted (for example across the building's wooden floors). In the developed technique, this is mainly achieved through the organic adhesion (by epoxy resins) of the CFRP mesh to specific steel devices (Fig. 1b) that will ensure the anchoring requirements [33].

3. Material characterization

The main mechanical characteristics of the materials constituting the strengthening solution (the CRFP reinforced mortar) were determined, along with those of the masonry test specimens used in the subsequent laboratory work. The most relevant mechanical properties, experimentally-determined, were those of the compressive strength and Young modulus, both for the coat mortar and for the equivalent-masonry material. As to the relevant mechanical properties of the reinforcing CFRP mesh material, the manufacturer specifications were of 4300 MPa and 1.75% for the tensile strength and ultimate strain, respectively.

The mortar matrix of the reinforced render material was mechanically characterized by uniaxial compression tests, where the compression strength and Young's modulus were determined. Mortars for non-structural rehabilitation of old masonry elements were considered the most suitable for the intended purposes, largely because of their mechanical and chemical compatibility. Several specimens of the sprayed mortars were prepared from which cylindrical core samples (Ø66 mm × 120 mm) were taken for further testing.

The mortar samples were tested according to the procedures defined in EN 12390:3 [34] at 28 days old (Table 1).

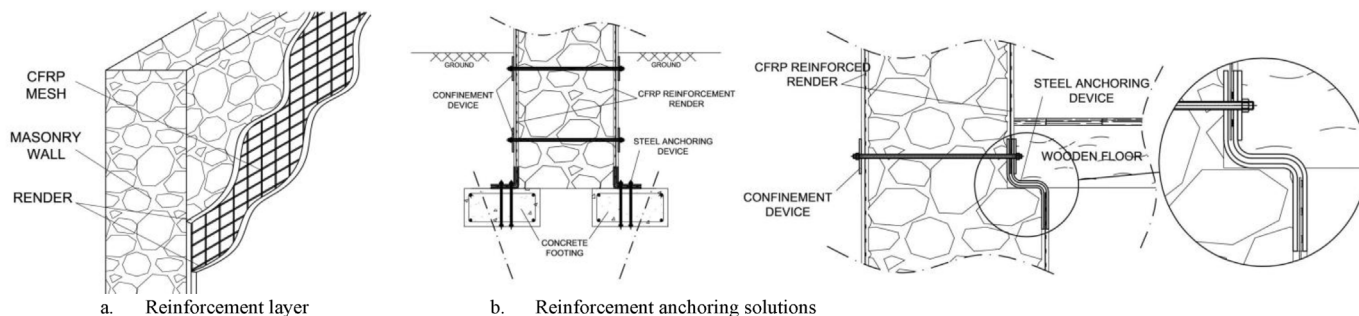


Fig. 1. Strengthening technique.



Fig. 2. Masonry wall specimens (left) and render mortar shotcrete operation (right).

Table 1
Coat mortar mechanical characterization (adapted from Ref. [28]).

Mortar solution	Uniaxial compressive strength		Young modulus	
	Average stress	Coefficient of variation	Average value	Coefficient of variation
Shotcreted non-cementitious mortar	4.81 MPa	6.27%	0.837 GPa	5.24%

As mentioned, masonry wall specimens were built to test the effect of the proposed strengthening solution. Manually manufactured masonry walls usually exhibit significant variability in terms of their mechanical and physical properties. For the required production of masonry wall specimens with lower variability, an equivalent-masonry material was developed that could be considered mechanically equivalent to the masonry typically found in old buildings.

The large number of masonry wall specimens (16) to be tested led to the development of a specific test material, here called equivalent-masonry, developed to replicate the relevant mechanical characteristics of typical rubble stone masonry. The equivalent-masonry is a material made from river sand, rich clay sand, coarse aggregate (gravel) and hydraulic lime, acting as binder. This material, produced in a batching plant, differs mechanically from real masonry because of its homogeneity in contrast to the different heterogeneities, both in height and thickness, of the latter material. However, as stated before, the macro mechanical characteristics are comparable. There was an initial study on the composition of the equivalent-masonry, varying the proportion of the constituents, and the final composition had mechanical properties similar to those of common rubble masonry.

It was mechanically characterized (Table 2) by uniaxial compression tests, according to EN 206:1 [35] and by tests to determine its

Table 2
Equivalent-masonry mechanical characterization.

Equivalent-masonry Id	Uniaxial compressive strength		Young modulus	
	Average stress	Coefficient of variation	Average value	Coefficient of variation
PSA_01	2.57 MPa	2.86%	2.11 GPa	0.10%
PSA_02	2.20 MPa	2.78%	2.10 GPa	0.08%
PSA_03	4.45 MPa	4.69%	–	–
PSA_04	3.67 MPa	2.37%	–	–
PSA_05	2.00 MPa	4.91%	3.46 GPa	7.46%
PSA_06	2.97 MPa	2.10%	7.02 GPa	2.85%
PSA_07	2.21 MPa	6.60%	6.21 GPa	0.47%

Young's modulus on cylinders measuring Ø150 mm × 300 mm (height), defined according to EN 12390:13 [36].

All tests were performed when the specimens were 28 days old, with samples collected from each equivalent-masonry manufactured. As PSA_03 and PSA_04 equivalent-masonry specimens were significantly stronger than PSA_01 and PSA_02, it was then decided to measure both the compressive strength and Young's modulus for the remaining specimens, PSA_05, PSA_06 and PSA_07. These equivalent-masonry specimens had compressive strengths similar to those of specimens PSA_01 and PSA_02. Regarding the Young's modulus, a higher dispersion of results was found, with values ranging between 2 GPa and 7 GPa.

As a whole, the former results present a scatter higher than expected. Nevertheless, the variability range of both experimentally-determined mechanical properties, compressive strength and Young modulus, is of the same order of magnitude of that could be expected in real masonry.

The subsequent tests were based on the assumption that the equivalent-masonry material is mechanically identical to common rubble stone masonry [37,38], both in terms of strength, deformability and adhesion to the reinforced render.

4. Description of the experimental setup

A specific experimental setup was conceived to perform quasi-static testing with reversed cycles of horizontal displacements on the equivalent-masonry specimens. This setup was developed to assess the seismic behaviour of specimens of masonry walls, both plain (unreinforced) and strengthened.

The geometry of the specimens had to be representative of the walls of old masonry buildings. Therefore, they consisted of an upper spandrel/enlarged pier, a pier and a bottom spandrel/enlarged pier (Fig. 3), all of these cast with the equivalent-masonry material. All masonry specimens were 40 cm thick, with shallow horizontal grooves. The grooves simulated the mortar joints, deepened during the preparation for the application of the strengthening layer to promote the adhesion [33,39].

A series of four reference tests were conducted first to characterize the non-reinforced behaviour of the masonry wall specimens (specimens EPR_A.100, EPR_B.200 and EPR_C.160, Table 3), with different test schemes (A to C, intermediate label in the designation) and vertical loading (suffix of the designation), presented in Figs. 4–6.

Test scheme A (specimen EPR_A.100, Fig. 4) did not prevent the rotation of the bottom spandrel/enlarged pier, inadvertently leading to premature rigid-body rocking of the whole specimen. This test scheme was discontinued and only one level of vertical load was considered (100 kN).

In the subsequent tests (with test schemes B and C) the bottom spandrel/enlarged pier displacements were restrained by a steel clamp,

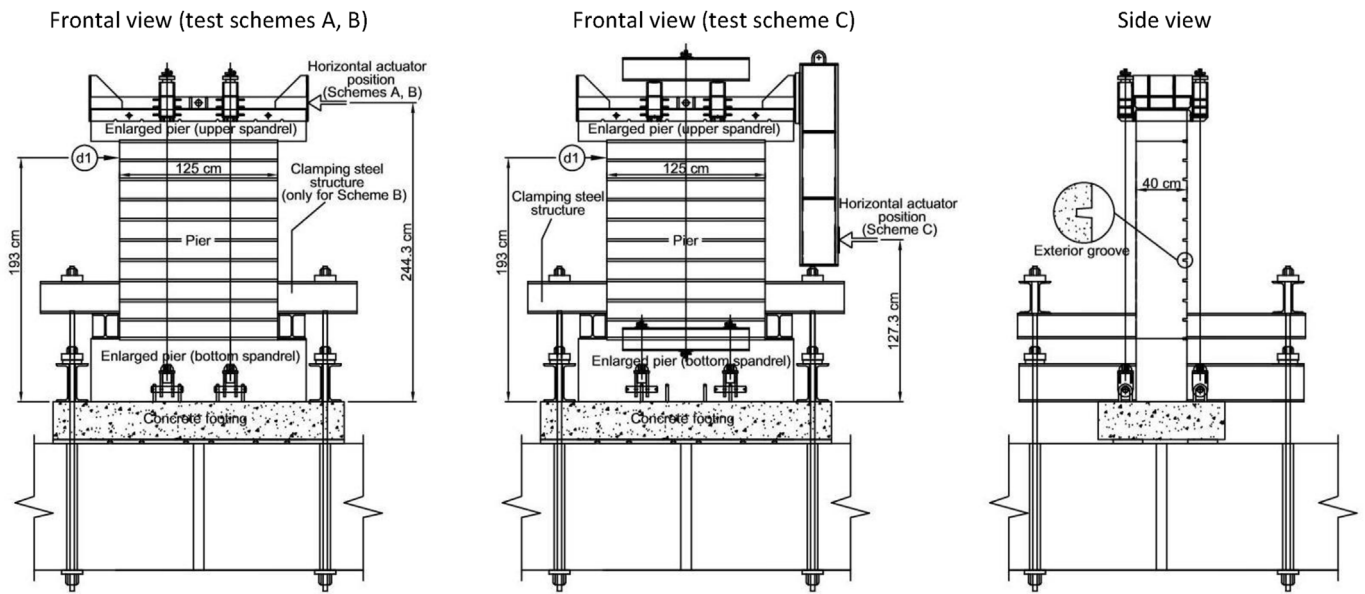


Fig. 3. Specimens geometry.

so as to prevent any undesirable rigid-body motion (sliding and rocking). In test scheme B (Fig. 5) the horizontal load was applied to the top of the wall, therefore leading to a predominantly in-plane bending behaviour mode. Two reference tests (EPR_B.100 and EPR_B.200 specimens) were conducted, varying the applied vertical load, as test scheme B was used for eight tests with strengthened specimens (EPN_B.1 to EPN_B.8).

The reduction of the height at which the horizontal load is applied has an effect of decreasing the shear span ratio, so that the behaviour of the wall is more dominated by shear, decreasing the bending contribution, as pretended by the modified test scheme C. Fig. 6 illustrates the static considerations that led to this test scheme, showing that despite the fact that the rotation of the top of the wall was not kinematically prevented, the bending moment diagram resembles that corresponding to the prevention of the top rotation. That figure also shows the limitations of the developed procedure, namely the fact that from a given value of the horizontal load $-V = \frac{N \cdot d}{h}$, related to the vertical load N and to the dimensions d and h of the wall – the bending moment diagram starts to differ from that of a rotationally restrained top wall and becomes progressively more similar to that of test scheme B.

The fact that test scheme C was not able to fully replicate the

behaviour of a wall panel (seen as part of a pier), rotationally restrained at storey level, is consistent with the observation that the spandrel and floor structure elements are not effectively connected to the pier walls in ancient loadbearing masonry buildings, providing instead a limited restraint to rotation to in-plane movements.

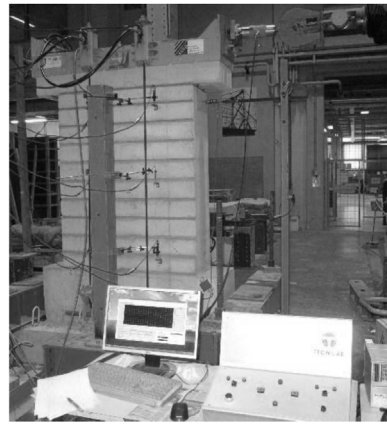
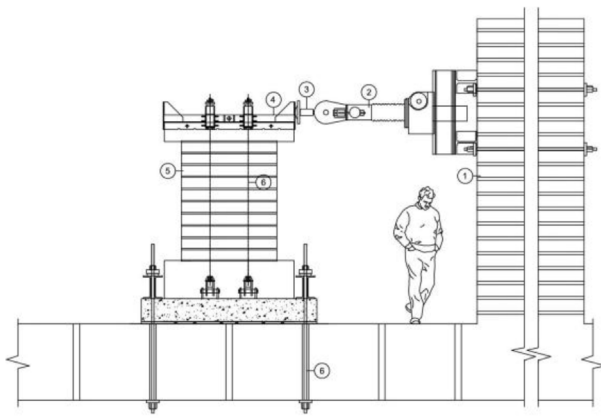
Only one reference test (EPR_C.160 specimen) was conducted using this scheme (Fig. 7), and four strengthened specimen tests were performed (EPN_C.1 to EPN_C.4), taking the same vertical load into consideration.

The test parameters considered were based on the main variables that should affect the behaviour of the masonry walls when subjected to horizontal loads, by varying the vertical load, the material composition of the CFRP mortar matrix and the presence of the confinement devices. The test specimens' dimensions and strengthening details are shown in Table 3.

The vertical load levels considered corresponded to the range of vertical stresses in old building masonry walls. Three different levels were considered for the pier cross-section: low (100 kN, 0.20 MPa in the specimen pier); intermediate (160 kN, 0.32 MPa in the specimen pier); and moderate (200 kN, 0.40 MPa in the specimen pier). The intermediate load level was considered only for test scheme C, while the

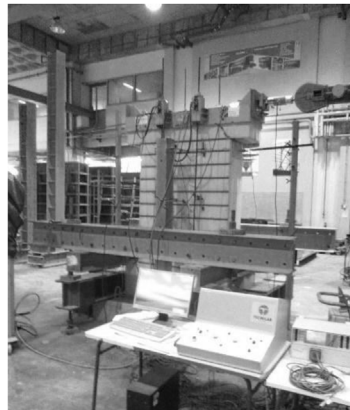
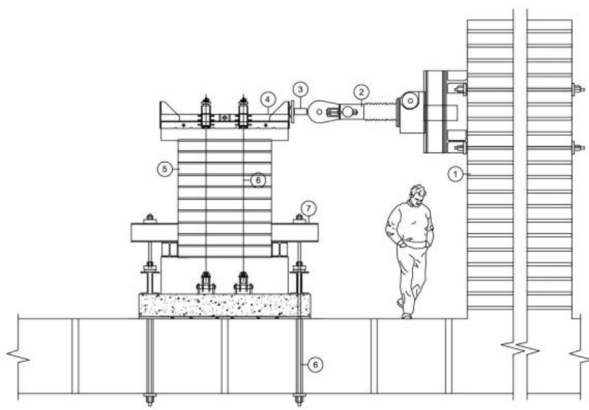
Table 3
Specimens' dimensions and strengthening details.

Specimen Id	Test scheme	Equivalent-masonry	Wall geometry		CFRP mesh	Confinement devices	Vertical load
			Pier	Spandrels			
EPR_A.100	A	PSA_01	156 cm	Bottom:	–	–	100 kN
EPR_B.100	B	PSA_01	(height)	50 cm			100 kN
EPR_B.200		PSA_06	X	(height)			200 kN
EPR_C.160	C	PSA_07	125 cm	X			160 kN
EPN_B.1	B	PSA_04	(width)	170 cm	2	Present (9 pairs on pier)	100 kN
EPN_B.2				(width)	crossed layers of a CFRP mesh		
EPN_B.3		PSA_03		Upper:	(200 g of carbon per m ² of mesh)		200 kN
EPN_B.4		PSA_05		25 cm			
EPN_B.5		PSA_04		(height)		Absent	100 kN
EPN_B.6				X			
EPN_B.7		PSA_02		170 cm			200 kN
EPN_B.8		PSA_03		(width))			
EPN_C.1	C	PSA_06				Present (9 pairs on pier)	160 kN
EPN_C.2		PSA_07					
EPN_C.3						Absent	
EPN_C.4							



- 1 Reaction wall
- 2 Mechanical actuator
- 3 Load cell
- 4 Steel helmet
- 5 Equivalent-masonry specimen
- 6 High strength steel bar

Fig. 4. Test scheme A.



- 1 Reaction wall
- 2 Mechanical actuator
- 3 Load cell
- 4 Steel helmet
- 5 Equivalent-masonry specimen
- 6 High strength steel bar
- 7 Restraining steel structure

Fig. 5. Test scheme B.

moderate load level was considered only for test scheme B. The reversed cyclic pseudo-static lateral loading was applied using a mechanical actuator (worm screw), coupled with a load cell that were connected to a steel helmet enveloping the upper spandrel. The horizontal displacement was imposed 244.3 cm above the concrete footing for test schemes A and B and 127.3 cm above that level for test scheme C (Fig. 3). The vertical load was applied by means of external post-tensioned High strength steel bars, attached between the steel helmet and the concrete footing (Figs. 4, 5 and 7). The magnitude of the applied vertical load was controlled by load cells and kept constant throughout the duration of the tests. Given the greater susceptibility to

sliding, test scheme C had additional steel elements that fixed the wall specimen to the reaction wall (Fig. 7).

The definition of the displacement history followed ASTM E2126:05 [40] specifications for cyclic alternate tests. Failure was conventionally defined when the horizontal load at a given cycle was less than 80% of the peak load achieved in the same direction in the preceding cycles. The loading history for test scheme C was slightly different since it had a group of alternate cycles, followed by a monotonic cycle to collapse.

The test assemblages are depicted in Fig. 8, with or without confinement devices. The test procedure was such that the reinforcing layer was anchored only after the vertical load had been applied in a similar

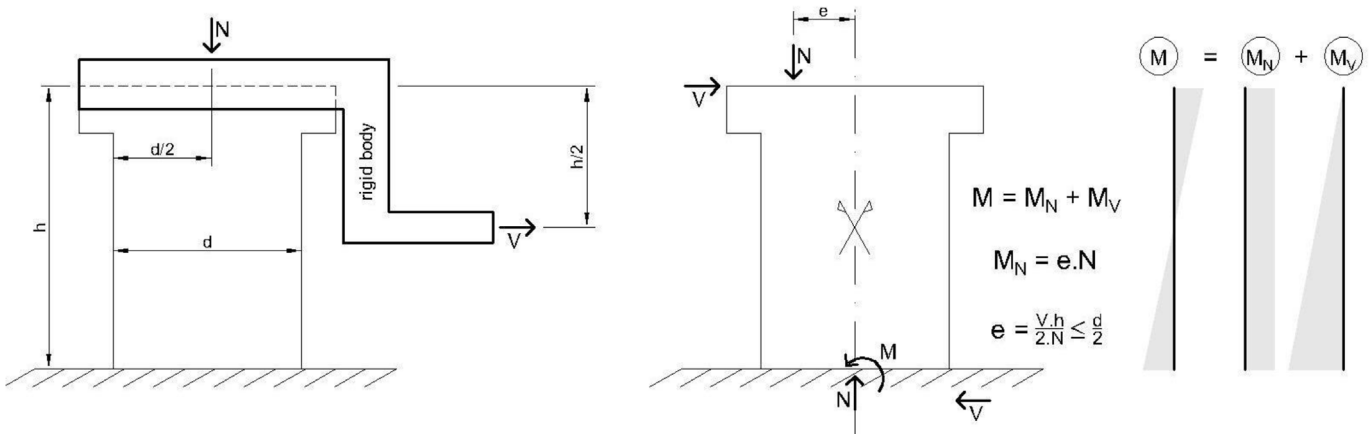


Fig. 6. Free-body diagram of the wall and bending moment distribution (Test Scheme C).

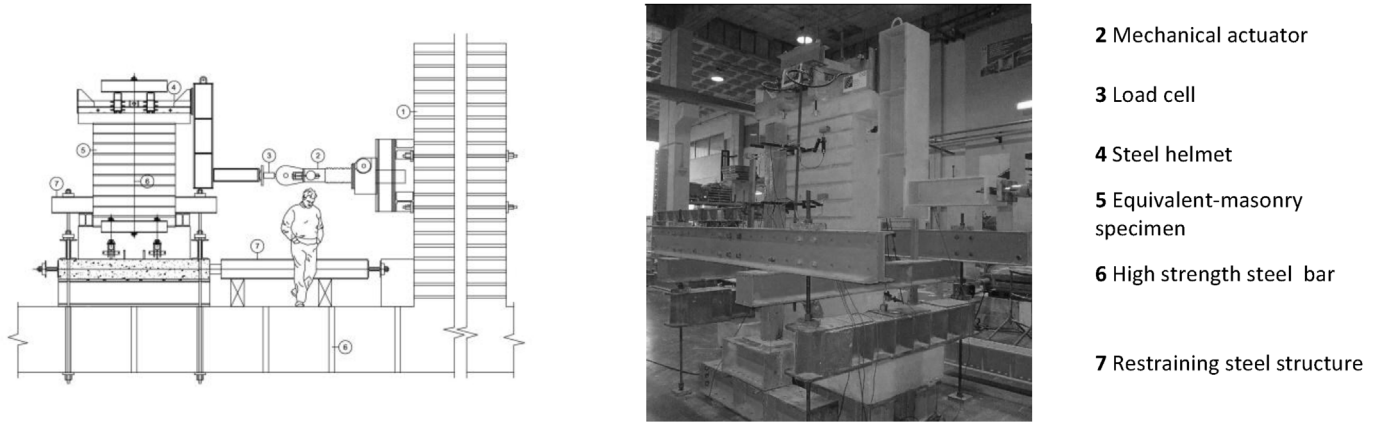
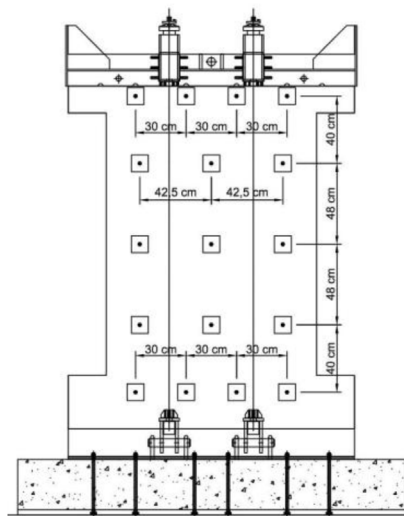
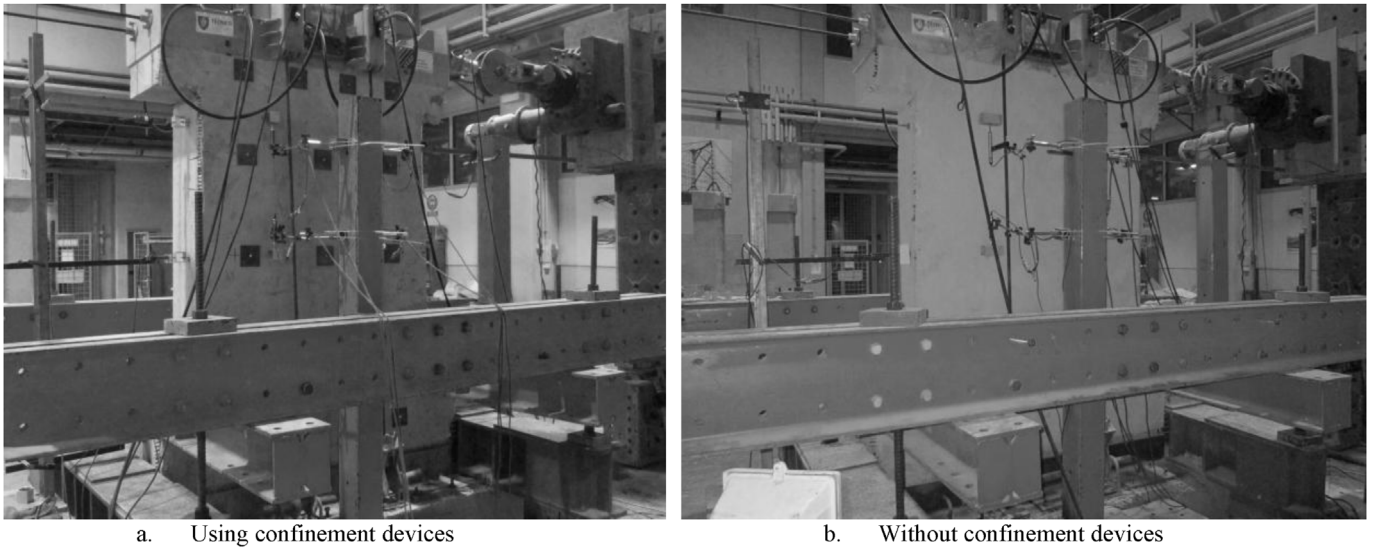


Fig. 7. Test scheme C.

manner to that of the application of the confinement devices.

5. Experimental results – test schemes A and B

Table 4 presents an overview of the test results with schemes A and B. The displacement presented there – displacement d1 – is the



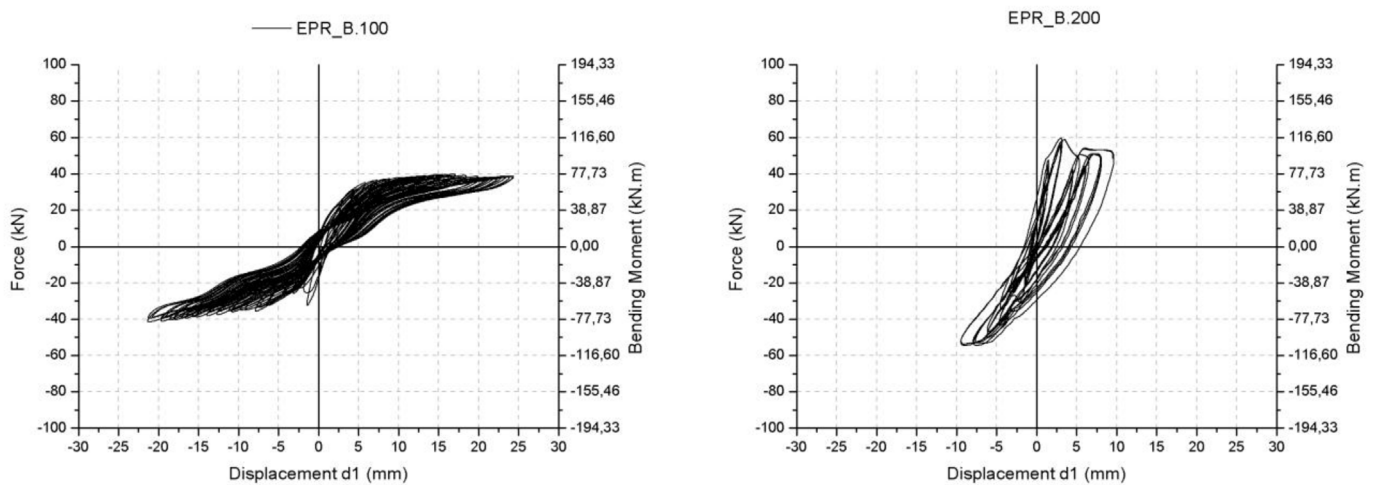
c. Confinement devices distribution

Fig. 8. Test assemblages.

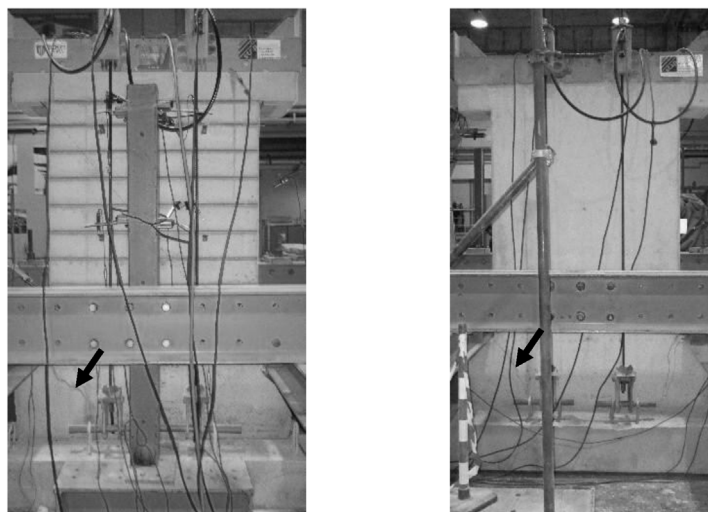
Table 4
Tests results overview (scheme A and B).

Specimen Id	Loading direction	Maximum load [kN]	Displacement at maximum load – <i>d1</i>	Drift at maximum load	Dissipated energy
EPR_A.100	PULL (+)	41.9 kN	10.0 mm (*)	0.51% (*)	4897 J
	PUSH (-)	41.0 kN	10.6 mm (*)	0.55% (*)	
EPR_B.100	PULL (+)	40.0 kN	17.4 mm (*)	0.90% (*)	8389 J
	PUSH (-)	42.1 kN	21.7 mm (*)	1.12% (*)	
EPR_B.200	PULL (+)	59.7 kN	3.0 mm (*)	0.16% (*)	–
	PUSH (-)	54.5 kN	7.4 mm (*)	0.38% (*)	
EPN_B.1	PULL (+)	67.6 kN	16.5 mm	0.85%	18557 J
	PUSH (-)	67.2 kN	13.5 mm	0.69%	
EPN_B.2	PULL (+)	72.3 kN	8.9 mm	0.46%	12610 J
	PUSH (-)	71.8 kN	17.0 mm	0.87%	
EPN_B.3	PULL (+)	90.5 kN	16.0 mm	0.82%	17094 J
	PUSH (-)	100.1 kN	12.7 mm	0.65%	
EPN_B.4	PULL (+)	94.1 kN	16.4 mm	0.84%	24344 J
	PUSH (-)	91.1 kN	20.8 mm	1.07%	
EPN_B.5	PULL (+)	70.3 kN	10.4 mm	0.54%	12170 J
	PUSH (-)	71.3 kN	9.0 mm	0.46%	
EPN_B.6	PULL (+)	68.6 kN	2.9 mm	0.15%	12865 J
	PUSH (-)	66.1 kN	16.5 mm	0.85%	
EPN_B.7	PULL (+)	85.1 kN	22.0 mm	1.13%	22637 J
	PUSH (-)	82.8 kN	11.6 mm	0.60%	
EPN_B.8	PULL (+)	90.2 kN	17.4 mm	0.90%	24981 J
	PUSH (-)	90.5 kN	16.9 mm	0.87%	

(*) The 80% of the peak load was not attained.



a. Load-displacement curves



b. Crack pattern (EPR_B.100 specimen)

Fig. 9. EPR_B.100 and EPR_B.200 test results.

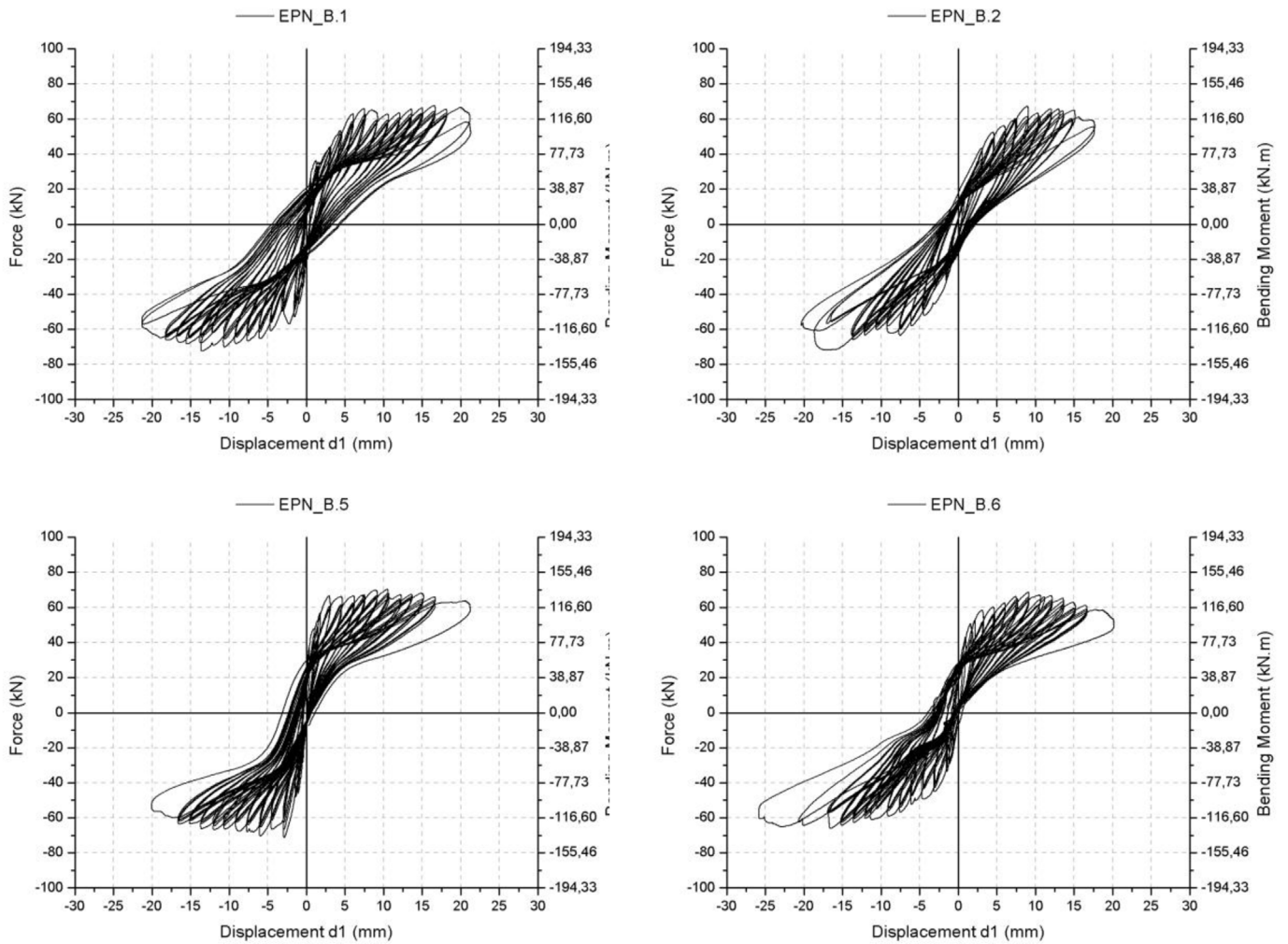


Fig. 10. Load displacement curves for the tests with low vertical load (100 kN) – Test scheme B.

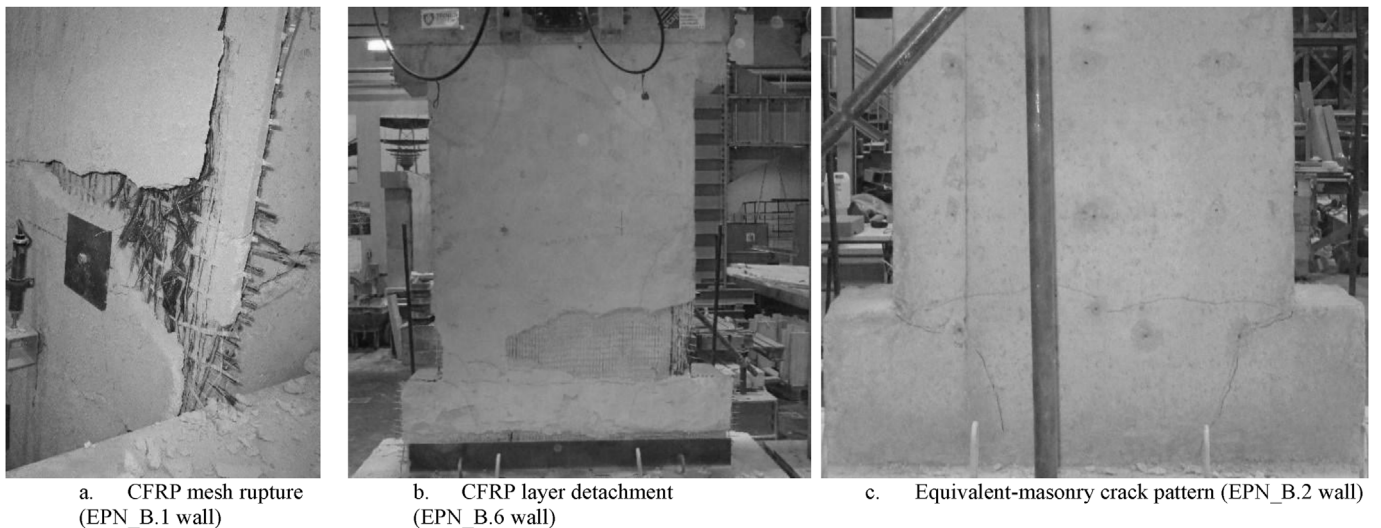


Fig. 11. Damage patterns for the tests with low vertical load (100 kN) – Test scheme B.

controlling displacement, measured 193 cm above the walls' concrete footing (Fig. 3).

As previously mentioned, test scheme A led to premature and non-representative failure since the specimen started to rotate in its own plane rather than showing the typical damage patterns of the in-plane

collapse mechanisms (diagonal or horizontal cracks).

The two reference tests with scheme B - EPR_B.100 and EPR_B.200 specimens – served as a way of assessing the lateral in-plane load-bearing capacity of the masonry walls (Fig. 9a) prior to strengthening. These tests had two different stages, before and after the development

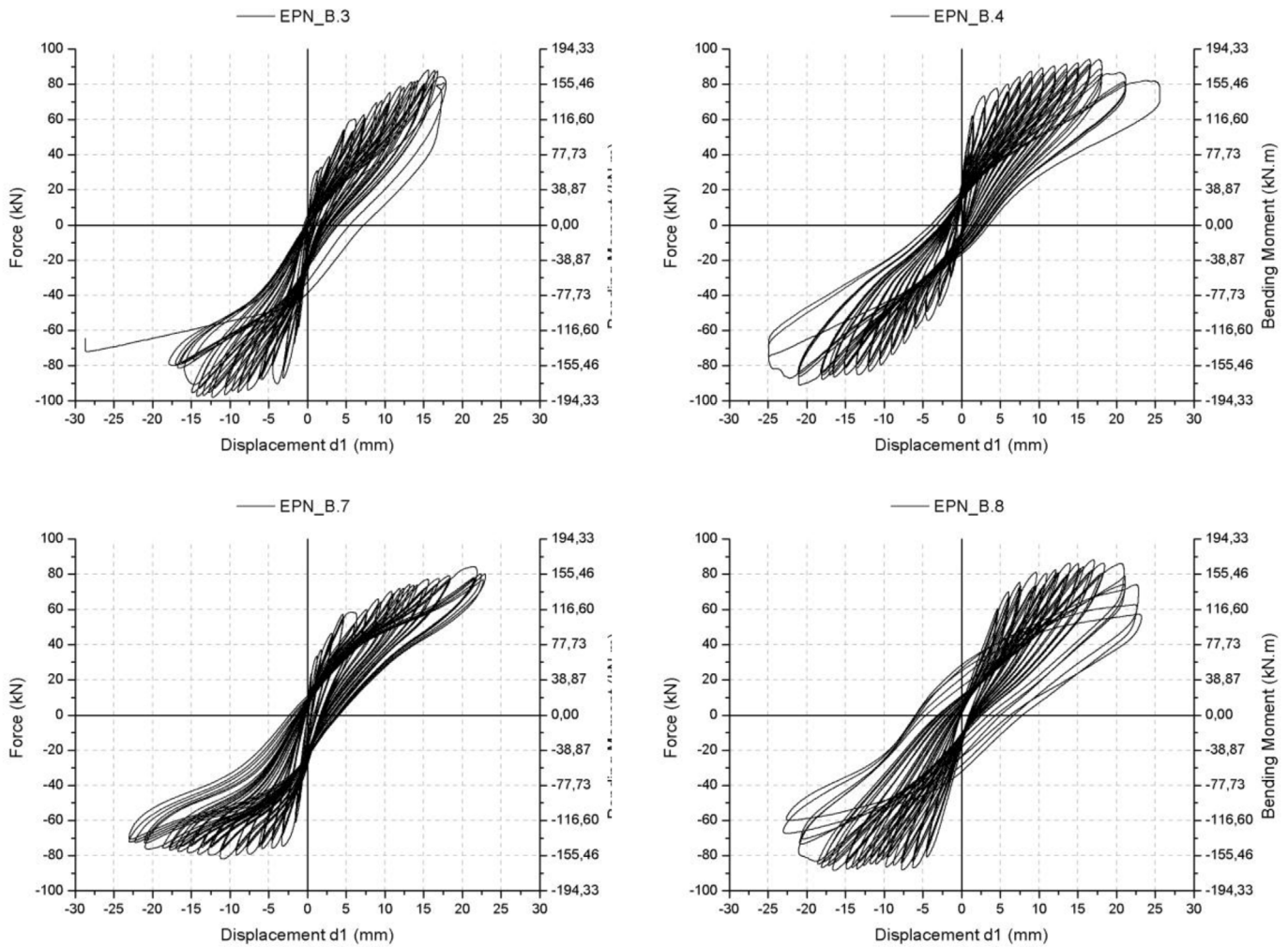


Fig. 12. Load displacement curves for the tests with moderate vertical load (200 kN).

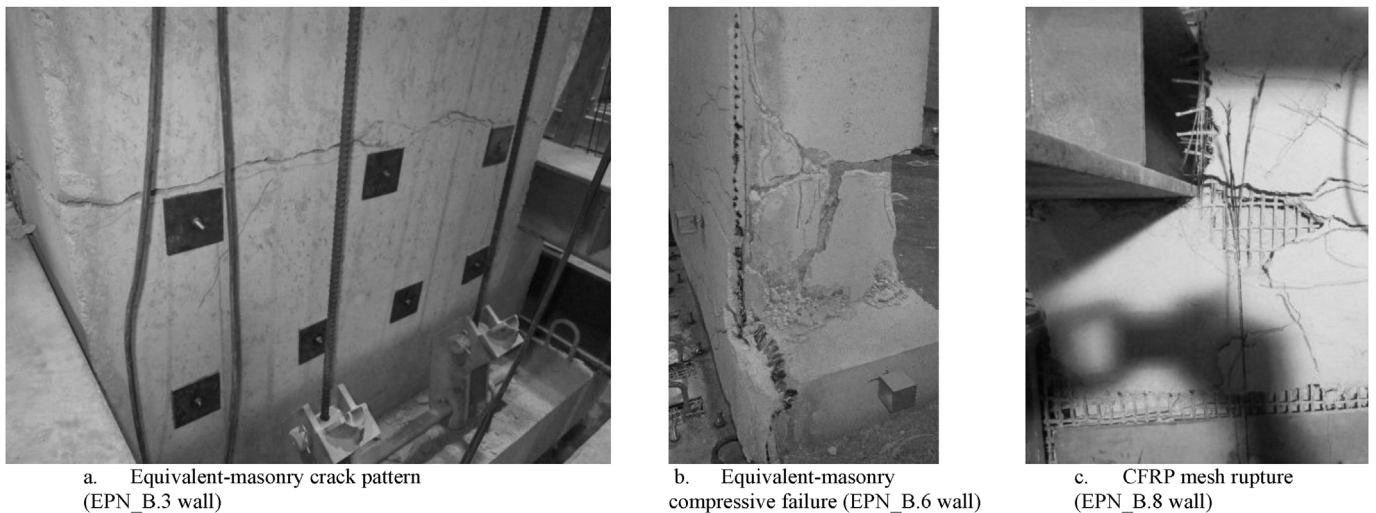


Fig. 13. Damage patterns for the tests with moderate vertical load (200 kN) – Test scheme B.

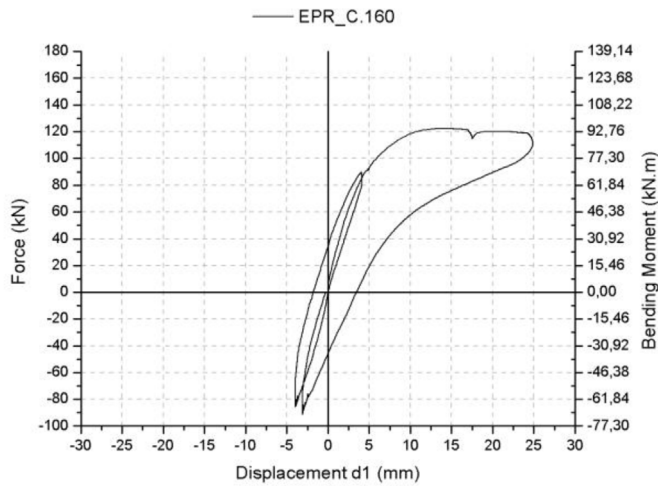
of cracks, which only appeared at the ends of the bottom spandrel (Fig. 9b). This damage pattern indicated the preponderance of the in-plane bending failure mechanism, rather than the shear induced collapse mechanism, which can be explained by the specimen geometry and the test scheme.

For the EPR_B.100 specimen the first bending crack developed for a

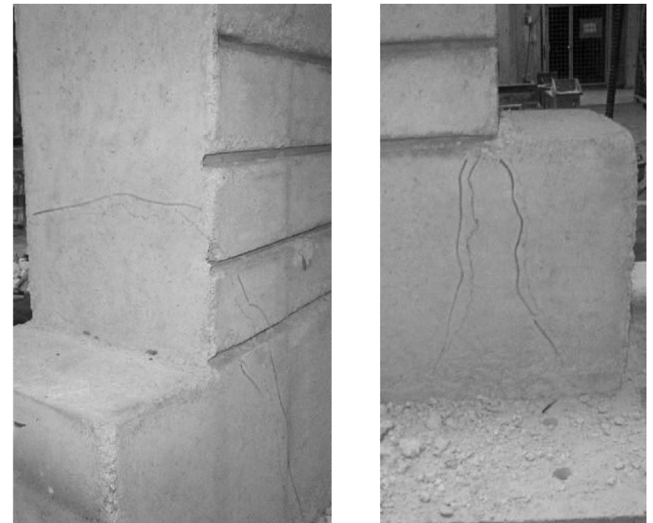
load force of 32.61 kN, associated with a significant decrease in stiffness, visible in the load-displacement curve. The EPR_B.100 specimen still showed some increase in resistance after cracking, exhibiting from then on a rigid-body behaviour (leading to a maximum load similar to that of the EPR_A.100 test, Table 4). This rigid-body behaviour after cracking was also shown by the EPR_B.200 specimen (Fig. 9a), without,

Table 5
Tests results overview (scheme C).

Specimen Id	Loading direction	Maximum load [kN]	Displacement at maximum load – d1	Drift at maximum load	Dissipated energy
EPR_C.160	PULL (+)	122.4 kN	14.0 mm	0,72%	954 J
EPN_C.1	PULL (+)	162.6 kN	20.2 mm	1,04%	2416 J
EPN_C.2	PULL (+)	147.5 kN	22.3 mm	1,15%	1853 J
EPN_C.3	PULL (+)	152.5 kN	15.3 mm	0,79%	1959 J
EPN_C.4	PULL (+)	150.9 kN	7.5 mm	0,39%	2249 J



a. Load displacement curves



b. Crack pattern

Fig. 14. EPR_C.160 test results.

however, showing any increase in resistance, leading to a premature failure mode.

The strengthened specimens with the lowest vertical load (EPN_B.1, EPN_B.2 and EPN_B.5, EPN_B.6) showed a considerable increase in resistance (Fig. 10, Table 4). However, this resistance increase was not associated with a significant rise in deformation capacity, as the maximum strength of all these specimens was achieved for displacements similar to those of the reference test (EPR_B.100 specimen).

In these tests the collapse was always due to the tear of the CFRP mesh (Fig. 11a), associated with a progressive decrease in the lateral bearing capacity. The CFRP mesh tear/rupture process developed from the ends to the pier, allowing for some ductility in the failure process. The confinement devices had a beneficial effect on the specimens' behaviour, as the CFRP layer detachment was more severe in the specimens without these devices (Fig. 11b). However, the collapse mode (involving the tear in the CFRP mesh) was not changed by the presence of such devices.

The crack pattern observed in the reference specimens kept appearing in these tests (bending cracks at the bottom spandrel, Fig. 11c), as the reinforcement ruptured long after the equivalent-masonry started to crack. Other cracks formed (horizontal cracks due also to in-plane bending), specific to the strengthened specimens, developing in a pattern similar to that of the reference tests.

Increasing the vertical load in strengthened specimens (EPN_B.3, EPN_B.4 and EPN_B.7, EPN_B.8, Fig. 12, Table 4) brought some differences to the results, notably that of increasing the maximum horizontal load when compared both to the equivalent reference specimen and to those of the strengthened specimens subjected to a lower vertical load. As was found for the specimens subjected to a lower vertical load, the aforementioned increase in strength was not matched by the deformation capacity.

For such a level of vertical load, the damage pattern suffered some

changes, while keeping the main aspects of the in-plane bending failure mechanisms.

There were additional horizontal cracks as well as new diagonal cracks at the ends of the piers (Fig. 13a). These new diagonal cracks arose from the excessive compressive states installed in the wall pier and were the main cause of collapse of specimen EPN_B.6 (Fig. 13b). The collapse of the other specimens resulted from the CFRP mesh rupture (Fig. 13c).

The EPN_B.3 and EPN_B.8 specimens were made of an equivalent-masonry (PSA_03) that was markedly stronger than a real masonry (Table 2). However, this did not seem to influence the behaviour of the tested walls since neither the damage patterns nor the strengths were remarkably different.

6. Experimental results – test scheme C

An overview of the test results with test scheme C is reported in Table 5. The displacement presented there – displacement d1 – represents the wall horizontal displacement at the same height as in the tests with schemes A and B (193 cm above the wall concrete footing, Fig. 3).

This scheme aimed to see how the horizontal load transmission by shear mechanisms influences the lateral bearing capacity of a strengthened wall. Nevertheless, the collapse mode was comparable to that of the other non-reinforced specimens, represented by the characteristic damage pattern (Fig. 14b). The fact that the collapse mechanism remained unchanged can be attributed to the high height/width ratio, susceptible to bending-dominated collapse mechanisms.

The lateral loading capacity of the strengthened specimens was increased (Figs. 14a and 15) with no significant enhancement in terms of the deformation capacity. The strengthened specimens ended up exhibiting very similar behaviours.

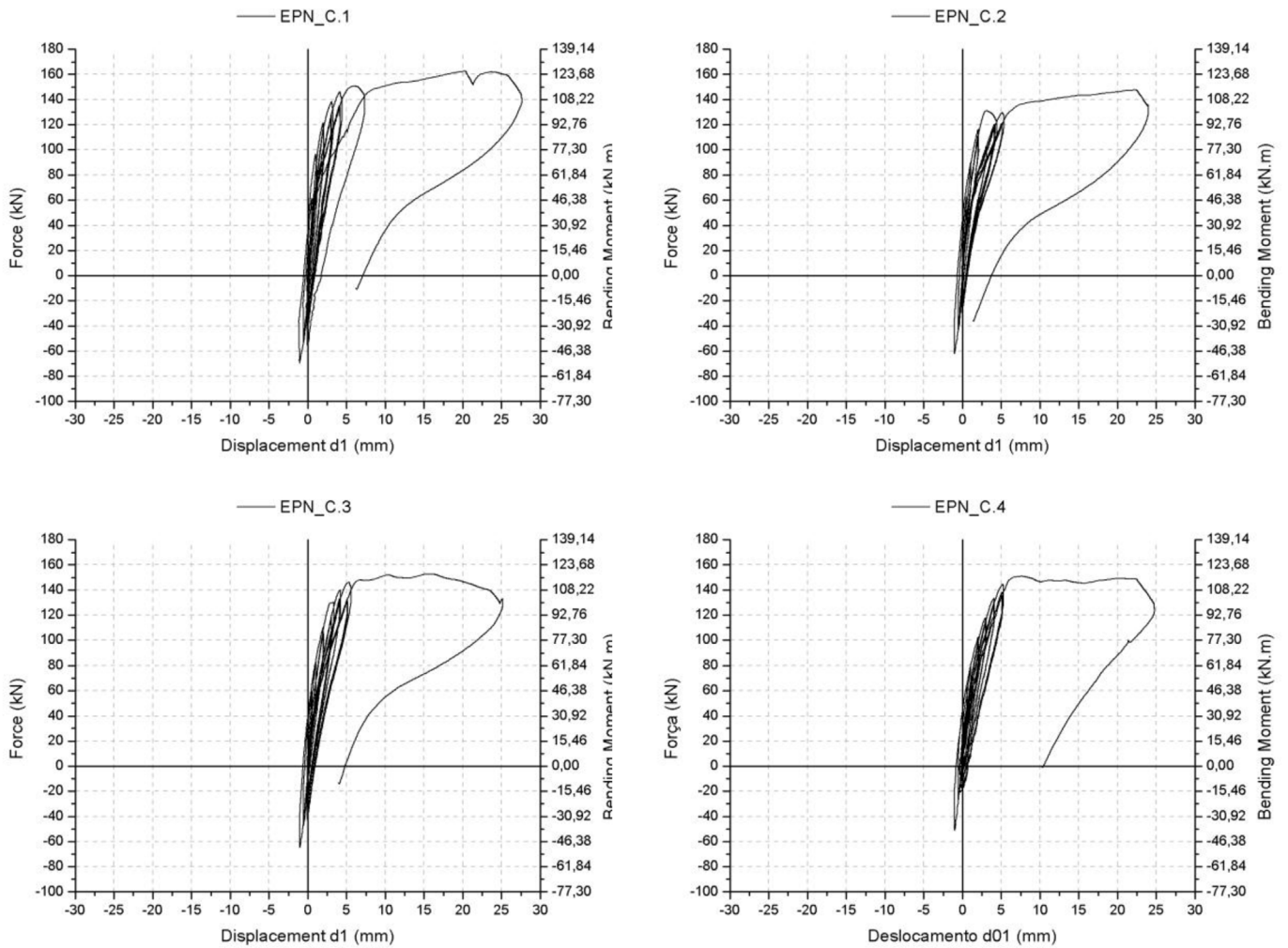
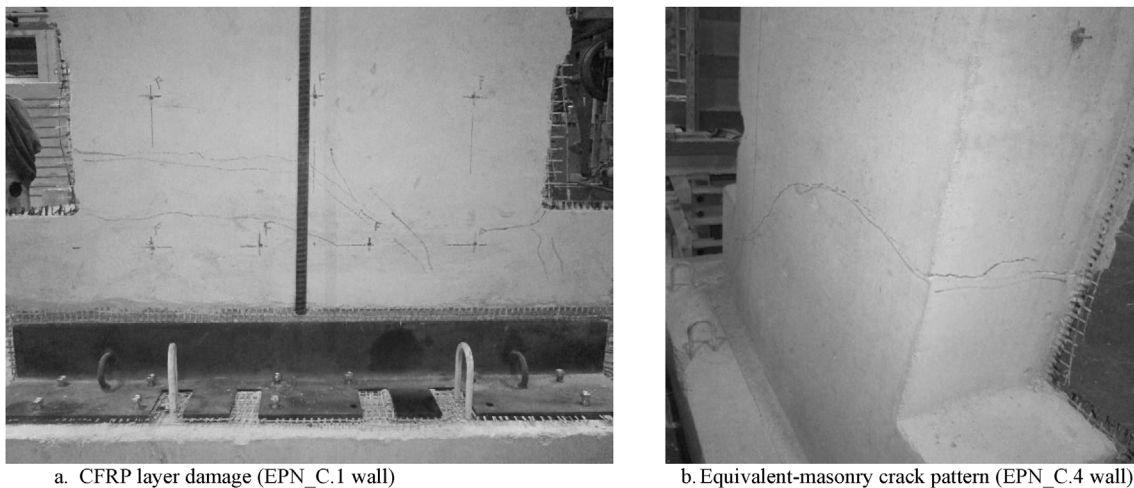


Fig. 15. Load displacement curves for the tests with scheme C.



a. CFRP layer damage (EPN_C.1 wall)

b. Equivalent-masonry crack pattern (EPN_C.4 wall)

Fig. 16. Damage patterns for the tests with the scheme C.

In contrast with what was found for the strengthened specimens tested with scheme B, the collapse of these specimens (EPN_C.1 to EPN_C.4) was not precipitated by the rupture of the CFRP mesh; it was instead caused by the formation of cracks due to the compression on the bottom spandrel (only on one side of the wall, given the monotonic loading). Before the formation of these cracks, other horizontal ones developed in the lower part of the wall pier (Fig. 16), in such a way that

eventually they intersected the cracks provoked by the compression states, thus precipitating the wall collapse.

Interestingly, in the absence of the rupture of the reinforcing material, the lateral strength of the specimens subjected to test scheme C was controlled by the compressive strength of the equivalent-masonry material.

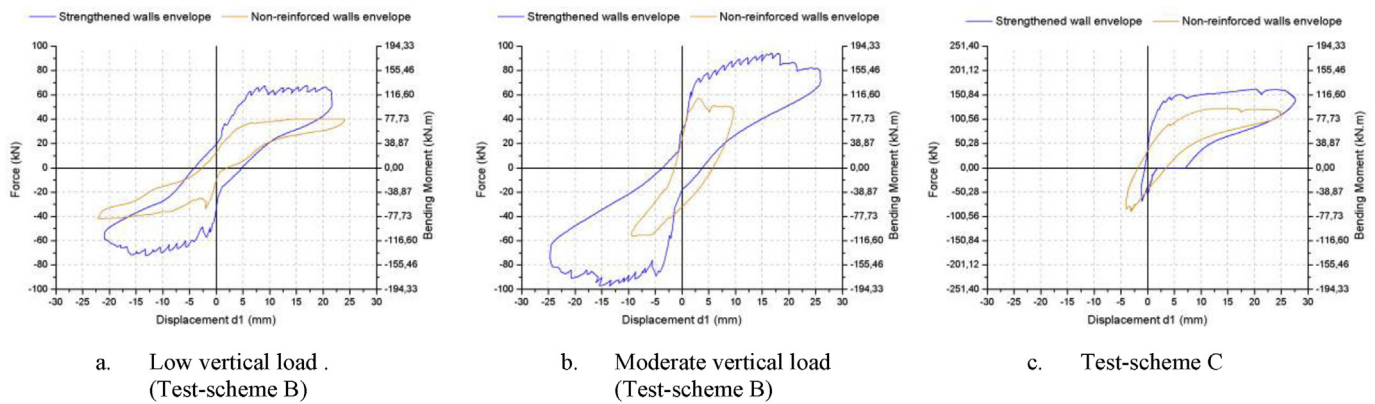


Fig. 17. Load-displacement curves envelopes.

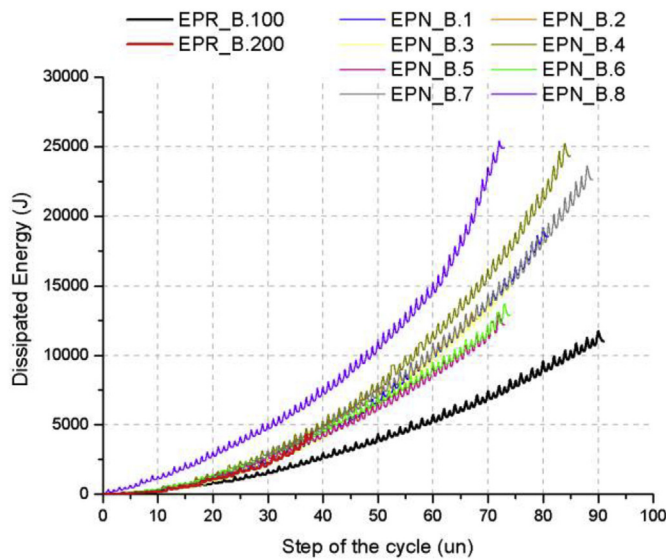


Fig. 18. Experimental dissipated energy results (tests with Scheme B).

7. Conclusions

The performed study shows that the developed strengthening technique has the potential to improve the behavioural parameters of the masonry walls of old buildings. The original purpose of overcoming the functional and structural incompatibilities shown by other strengthening techniques was achieved since the mechanical behaviour of the strengthened walls was significantly improved in terms of strength, damage dissemination and energy dissipation, as the extensive experimental work demonstrated.

The observed damaged patterns for the strengthened specimens matched the characteristic behaviour of walls when subjected to in-plane loading, even when no shear dominated failure modes occurred.

The strengthened specimens exhibited increased lateral strength, irrespective of the vertical load level (Fig. 17). The strength also increased for higher vertical loads, but it started to be dependent on the compressive strength of the wall. The overall stiffness of the wall seemed unchanged by the strengthening technique (Fig. 17).

The integrity of a structure when subjected to an earthquake depends on the ability of that same structure to dissipate the energy input from the ground motion. The estimation of the energy input is not straightforward but, unquestionably, the increase in the capability of dissipating energy, through stable non-linear behaviour, reduces the seismic risk and vulnerability of a given structure. The experimental tests can serve to assess the energy dissipation capabilities for different structural details. The energy dissipated in a cycle can be calculated as

the area that the hysteretic loop encloses in the corresponding masonry wall “load vs. displacement at the load-point” plot. The cumulative energy dissipated by each of the specimens during the reversed cyclic load test was calculated by summing up the energy dissipated in consecutive load-displacement loops throughout the tests. The energy dissipation capacity was significantly enhanced with the strengthening technique as shown in Fig. 18 for the test scheme B. This increase in the energy dissipation can be attributed to the increased strength and the more disseminated cracking pattern.

The encouraging results of this experimental programme must be followed by numerical studies (enabling the extrapolation of the results), ultimately leading to the derivation of design and detailing rules that could serve to guide the application of the strengthening technique.

The effects of this strengthening technique at the design stage could be considered through the derivation of the modified formulae for the most commonly masonry walls in-plane failure modes (i.e., sliding shear, diagonal cracking and rocking/toe crushing), in the same way as presented in Ref. [41].

Acknowledgments

The authors gratefully acknowledge STAP, S.A, promoter of the R&D project “RehabToolBox”, sponsored by FEDER through the POR Lisboa – QREN – Sistemas de Incentivos I&DT, for allowing the disclosure of the data presented in this article.

The authors gratefully acknowledge S&P, S.A’s participation in the same R&D Project.

The authors gratefully acknowledge the funding by Ministério da Ciência, Tecnologia e Ensino Superior, FCT, Portugal, under grant SFRH/BD/79339/2011.

References

- [1] Guerreiro J, Ferreira J, Proença J, Gago A. Strengthening of old masonry walls for out-of-Plane seismic loading with a CFRP reinforced render. *Exp Tech* 2018 <https://doi.org/10.1007/s40799-018-0239-0>.
- [2] Tomazevic M. *Earthquake-resistant design of masonry buildings*. London, England: Imperial College Press; 1999. p. 2. Series on innovation in structures and construction ISBN 1860940668.
- [3] Gattesco N, Boem I. Out-of-plane behavior of reinforced masonry walls: experimental and numerical study. *Compos B Eng* 2017;128:39–52 <https://doi.org/10.1016/j.compositesb.2017.07.006>.
- [4] Tesei C, Ventura G. A unilateral nonlocal tensile damage model for masonry structures. *21st european conference on fracture*. vol. 2. 2016. p. 2690–7. Catania, Italy.
- [5] Bosiljkov V, Page A, Zarnic R. Performance based studies on in-plane loaded unreinforced masonry walls. *Masonry International* 2003;16(2):39–50. ISSN: 0950-2289.
- [6] Calderini C, Cattari S, Lagomarsino S. In-plane strength of unreinforced masonry piers. *Earthq Eng Struct Dynam* 2009;38:243–67 <https://doi.org/10.1002/eqe.860>.
- [7] Lagomarsino S, Penna A, Galasco A, Cattari S. TREMURI program: an equivalent frame model for the nonlinear seismic analysis of masonry buildings. *Eng Struct*

- 2013;56:1787–99<https://doi.org/10.1016/j.engstruct.2013.08.002>.
- [8] Mrozek M, Mrozek D, Wawrzyniak A. Numerical analysis of selection of the most effective configuration of CFRP composites reinforcement of masonry specimens. *Compos B Eng* 2015;70:189–200<https://doi.org/10.1016/j.compositesb.2014.11.016>.
- [9] Mayes R, Clough R. *State-of-the-art in seismic shear strength of masonry - an evaluation and review* Berkeley, California, USA: Earthquake Engineering Research Center (California University); 1975. Report N° EERC 75–21.
- [10] Magenes G, Calvi M. In-plane seismic response of brick masonry walls. *Earthq Eng Struct Dynam* 1997;26. [http://dx.doi.org/10.1002/\(SICI\)1096-9845\(199711\)26:11<1091::AID-EQE693>3.0.CO;2-6](http://dx.doi.org/10.1002/(SICI)1096-9845(199711)26:11<1091::AID-EQE693>3.0.CO;2-6). 1091–112.
- [11] Marcarì G, Manfredi G, Prota A, Pecce M. In-plane shear performance of masonry panels strengthened with FRP. *Compos B Eng* 2007;38:887–901<https://doi.org/10.1016/j.compositesb.2006.11.004>.
- [12] Triantafillou T. Strengthening of masonry structures using epoxy-bonded FRP laminates. *J Compos Construct* 1998;2:96–104[https://doi.org/10.1061/\(ASCE\)1090-0268\(1998\)2:2\(96\)](https://doi.org/10.1061/(ASCE)1090-0268(1998)2:2(96)).
- [13] Dizhur D, Griffith M, Ingham J. Out-of-plane strengthening of unreinforced masonry walls using near surface mounted fibre reinforced polymer strips. *Eng Struct* 2014;59:330–43<https://doi.org/10.1016/j.engstruct.2013.10.026>.
- [14] Milani G, Shehu R, Valente R. Possibilities and limitations of innovative retrofitting for masonry churches: advanced computations on three case studies. *Construct Build Mater* 2017;147:239–63<https://doi.org/10.1016/j.conbuildmat.2017.04.075>.
- [15] Ramaglia G, Lignola P, Prota A. Collapse analysis of slender masonry barrel vaults. *Eng Struct* 2016;117:86–100<https://doi.org/10.1016/j.engstruct.2016.03.016>.
- [16] Valluzzi M, Tinazzi D, Modena C. Shear behavior of masonry panels strengthened by FRP laminates. *Construct Build Mater* 2002;16:409–16[https://doi.org/10.1016/S0950-0618\(02\)00043-0](https://doi.org/10.1016/S0950-0618(02)00043-0).
- [17] Cecchi A, Milani G, Tralli A. In-plane loaded CFRP reinforced masonry walls: mechanical characteristics by homogenisation procedures. *Compos Sci Technol* 2004;64:2097–112<https://doi.org/10.1016/j.compscitech.2004.03.009>.
- [18] Carozzi F, Bellini A, D'Antino T, Felice G, Focacci F, Hojdis L, Laghi L, Lanoye E, Micelli F, Panizza M, Poggia C. Experimental investigation of tensile and bond properties of Carbon-FRCM composites for strengthening masonry elements. *Compos B Eng* 2017;128:100–19<https://doi.org/10.1016/j.compositesb.2017.06.018>.
- [19] Aiello M, Sciolti S. Bond analysis of masonry structures strengthened with CFRP sheets. *Construct Build Mater* 2006;20: 90–00 <https://doi.org/10.1016/j.conbuildmat.2005.06.040>.
- [20] Luccioni B, Rougier V. In-plane retrofitting of masonry panels with fibre reinforced composite materials. *Construct Build Mater* 2011;25:1772–88<https://doi.org/10.1016/j.conbuildmat.2010.11.088>.
- [21] Papanicolaou C, Triantafillou T, Lekka M. Externally bonded grids as strengthening and seismic retrofitting materials of masonry panels. *Construct Build Mater* 2011;25:504–14<https://doi.org/10.1016/j.conbuildmat.2010.07.018>.
- [22] Ismail A, Ingham J. In-plane and out-of-plane testing of unreinforced masonry walls strengthened using polymer textile reinforced mortar. *Eng Struct* 2016;118:167–77<https://doi.org/10.1016/j.engstruct.2016.03.041>.
- [23] Bilotta A, Ceroni F, Lignola G, Prota A. Use of DIC technique for investigating the behaviour of FRCM materials for strengthening masonry elements. *Compos B Eng* 2017;129:251–70<https://doi.org/10.1016/j.compositesb.2017.05.075>.
- [24] D'Ambrisi A, Feo L, Focacci F. Experimental and analytical investigation on bond between Carbon-FRCM materials and masonry. *Compos B Eng* 2013;46:15–20<https://doi.org/10.1016/j.compositesb.2012.10.018>.
- [25] Carozzi F, Bellini A, D'Antino T, Felice G, Focacci F, Hojdis L, Laghi L, Lanoye E, Micelli F, Panizza M, Poggi C. Experimental investigation of tensile and bond properties of Carbon-FRCM composites for strengthening masonry elements. *Compos B Eng* 2013;46:15–20<https://doi.org/10.1016/j.compositesb.2017.06.018>.
- [26] Carozzi F, Poggi C. Mechanical properties and debonding strength of Fabric Reinforced Cementitious Matrix (FRCM) systems for masonry strengthening. *Compos B Eng* 2015;70:215–30<https://doi.org/10.1016/j.compositesb.2014.10.056>.
- [27] Feo L, Luciano R, Misseri G, Rovero L. Irregular stone masonries: analysis and strengthening with glass fibre reinforced composites. *Compos B Eng* 2016;92:84–93<https://doi.org/10.1016/j.compositesb.2016.02.038>.
- [28] Guerreiro J, Proença M, Ferreira J, Gago A. Bonding and anchoring of a CFRP reinforced render for external strengthening of old masonry buildings. *Construct Build Mater* 2017;155:56–64<https://doi.org/10.1016/j.conbuildmat.2017.08.043>.
- [29] Colen I, Brito J, Branco F. In situ adherence evaluation of coating materials. *Exp Tech* 2008;33:51–60<https://doi.org/10.1111/j.1747-1567.2008.00372.x>.
- [30] Mazzotti C, Ferracuti B, Bellini AE. Experimental bond tests on masonry panels strengthened by FRP. *Compos B Eng* 2015;80:223–37<https://doi.org/10.1016/j.compositesb.2015.05.019>.
- [31] Giuffrè A. *Sicurezza e conservazione dei centri storici in area sismica, il caso Ortigia*. Bari, Italy: Editoria Laterza; 1993. ISBN: 9788842042501.
- [32] Giaretton M, Dizhur D, Porto F, Ingham Z. Constituent material properties of New Zealand unreinforced stone masonry buildings. *Journal of Building Engineering* 2015;4:75–85<https://doi.org/10.1016/j.job.2015.08.005>.
- [33] Gago A, Proença A, Cardoso J, Coias V, Paula R. Seismic strengthening of stone masonry walls with glass fiber reinforced polymer strips and mechanical anchorages. *Exp Tech* 2009;35:45–53<https://doi.org/10.1111/j.1747-1567.2009.00544.x>.
- [34] EN 12390:3. *Testing hardened concrete; Part 3: compressive strength of test specimens*. 2009.
- [35] EN 206:1. *Concrete. Specification, performance, production and conformity*. 2000.
- [36] EN 12390:13. *Testing hardened concrete. Part 13: determination of secant modulus of elasticity in compression*. 2013.
- [37] NTC08. *Ministero delle Infrastrutture e dei Trasporti – nuove Norme Tecniche per le Costruzioni*. 2008. Italian Ministry of Infrastructures and Transportation. G.U. n.29 – S.O. n.30, February, 4th 2008, Rome, Italy (in Italian).
- [38] Milosevic J, Gago A, Lopes M, Bento R. Experimental assessment of shear strength parameters on rubble stone masonry specimens. *Construct Build Mater* 2013;47:1372–80<https://doi.org/10.1016/j.conbuildmat.2013.06.036>.
- [39] Sassoni E, Sarti V, Bellini A, Mazzotti C, Franzoni E. The role of mortar joints in FRP debonding from masonry. *Compos B Eng* 2018;135:166–74<https://doi.org/10.1016/j.compositesb.2017.10.021>.
- [40] ASTM E2126:05. *Standard test methods for cyclic (reversed) load test for shear resistance of walls for buildings*. 2005.
- [41] Proença J, Gago A, Chaves F. A simplified methodology for the seismic assessment of masonry buildings with RC slabs. *Bull Earthq Eng* 2018;16:377–95<https://doi.org/10.1007/s10518-017-0198-3>.